Mantle wedge olivine modifies slab-derived fluids: Implications for fluid transport from slab to arc magma source

Citation for published version:
De hoog, JCM, Clarke, E & Hattori, K 2023, 'Mantle wedge olivine modifies slab-derived fluids: Implications for fluid transport from slab to arc magma source', *Geology*. https://doi.org/10.1130/G51169.1

Digital Object Identifier (DOI):
10.1130/G51169.1

Link:
Link to publication record in Edinburgh Research Explorer

Document Version:
Peer reviewed version

Published In:
Geology

Mantle wedge olivine modifies slab-derived fluids: implications for fluid transport from slab to arc magma source

Jan C.M. De Hoog[1], Eleri R. Clarke[1], and Keiko H. Hattori[2]

[1] Grant Institute, School of GeoSciences, The University of Edinburgh, EH9 3FE, United Kingdom

[2] Dept. of Earth and Environmental Sciences, University of Ottawa, ON, K1N 6N5, Canada

ABSTRACT

Boron is an effective tracer of fluid processes in subduction zones. High B and δ^{11}B in arc magmas requires efficient B transfer from the slab to magma source regions. The Higashi-akaishi (HA) metaperidotite body in the Sanbagawa high-pressure belt, Japan, is composed of locally serpentinised mantle wedge peridotites exhumed in a subduction channel. Cores of coarse-grained primary mantle olivine have 1-4 µg/g B, enriched compared to typical mantle olivine, and δ^{11}B of -10 to -1‰, consistent with incorporation of fluids from dehydrating slab at ca. 90-120 km depth. Rims of primary mantle olivine as well as olivine neoblasts, have even higher B (5-20 µg/g) and higher δ^{11}B (-8 to +2 ‰) due to incorporating slab fluids at depths of ca. 70-100 km. Antigorite, formed below 650 °C, shows comparable δ^{11}B and B contents as olivine rims. The data shows that olivine is capable of scavenging significant amounts of B from fluids by diffusion and recrystallisation at sub-arc pressures and temperatures. Considering the large amount of olivine in the mantle wedge, transport of slab-derived material to magma sources requires processes with minimal interaction with mantle peridotite, such as intensely channelized fluid flow or ascent of mélange diapirs, and limited porous fluid flow.

INTRODUCTION

Large amounts of volatile and fluid-mobile elements (FME; B, Li, halogens) are subducted into the Earth's interior along convergent margins. Part of this FME cargo is returned to the surface by arc magmas, but large uncertainties still exist about the mode of transport of slab-derived material to magma sources. Models include metasomatism by fluids and/or melts derived from the slab beneath the arc (Ayers, 1998), down-dragging of mantle wedge serpentinites followed by their dehydration beneath the volcanic front (Hattori and Guillot, 2003), and the diapiric ascent of mélange from the interface between subducting slab and mantle wedge (Marschall and Schumacher, 2012).

Boron is an effective tracer of fluids in subduction zones, due to high B concentrations in surface reservoirs, low concentration in the mantle, high solubility in aqueous fluids and large isotope fractionations, and has provided important constraints on subduction-related fluid sources to arc magmas (De Hoog and Savov, 2018).

Here we present in-situ B isotope data of partially serpentinised peridotites from the Higashi-akaishi (HA) ultramafic body, Sanbagawa Complex, Japan, which represent mantle wedge material metasomatized at sub-arc depths. Data was collected by Secondary Ion Mass Spectrometry at the Edinburgh Ion Microprobe Facility using matrix-matched standards for calibration (see Electronic Supplement for analytical details). Small analytical beam size (<30 μm) compared to olivine grain size allowed the measurement of core-rim zoning of B contents and its isotope compositions. δ^{11}B values and high B in olivine compared to typical primary mantle olivine are consistent with infiltration of slab-derived fluids at sub-arc depths. The high affinity of B for olivine indicates that B in slab-derived fluids would be depleted efficiently in the mantle wedge at sub-arc conditions. Thus, transport of FME to arc magma sources requires minimal interaction of fluids with mantle wedge peridotites.

GEOLOGICAL BACKGROUND

The HA ultramafic body in the Sanbagawa belt, Japan, is a several kilometer-sized body composed of partially serpentinised peridotites and wehrlites with lenses of garnet-bearing lithologies and chromitites (Fig. 1). The body contains mantle wedge peridotites including cumulates and residual mantle (Hattori et al., 2010) that were fluxed by slab-derived fluids at high pressure in a subduction channel (Aoya et al., 2013; Guild et al., 2020; Hattori et al., 2010; Mizukami and Wallis, 2005; Sumino et al., 2007), and may ultimately have been derived by delamination from the lithospheric mantle section of the overriding plate (Guild et al., 2020).

The rocks record four stages of deformation (D1-D4; Mizukami and Wallis, 2005; Wallis et al., 2011). The first stage (D1) resulted in preferred orientation of coarse-grained olivine under low H_2O activity, and high T (715-800°C) and P (2.1-2.6 GPa) (Enami et al., 2004; Guild et al., 2020).

The second stage (D2) caused dynamic recrystallisation and grain size reduction of olivine (D2a), forming neoblasts during near isothermal pressure increase up to 3-4 GPa (Enami et al., 2004), followed by decompression and cooling. During this stage, antigorite formed after cooling below 650°C (D2b), which mostly affected the outer few 100 meters of the body (Fig. 1).

Exhumation in the subduction channel resulted in new foliation defined by olivine neoblasts and antigorite (D3), and amalgamation with the nearby supracrustal Besshi Unit at around 1 GPa and 600°C. Finally, further exhumation (D4) of the HA body as part of the Sanbagawa belt let to influx of crustal fluids under greenschist-facies to form lizardite veining (Mizukami et al., 2012).

The samples used in this study (**Fig. 1**) are five variably serpentinised, residual metadunites previously described in Hattori et al. (2010). All samples contain abundant primary (partially recrystallized) mantle olivine (Fo90-94, NiO 0.28-0.48 wt%, MnO 0.10-0.16 wt%) and 1-5% chromite (Cr# >0.7, TiO_2 <0.4 wt%). Three samples (HSS73, HC104, HSS46) contain abundant platy antigorite with high Mg# (96-98%) and 0.2-1.0 wt% Al_2O_3, whereas HC87 contains minor antigorite (<2%), and HC123 contains rare chlorite (<0.1%) but no antigorite. Late-stage veinlets of lizardite show variable Mg# (92-97) and low Al_2O_3 (<0.01 wt%). More detailed sample descriptions are in the Electronic Supplement. Serpentine species were not determined as part of this study, but distinction of antigorite vs. lizardite was based on petrographic examination and consistent with the observations of HA rocks by previous researchers (Mizukami et al., 2012; Wallis et al., 2011).

RESULTS

Olivine has a wide range in B contents (0.4-27 µg/g), which vary among grains in individual samples (**Figs. 2, 3**). Only sample HC123, which lacks antigorite but has trace amounts of chlorite, has olivine with comparatively low B contents (1.2-5 µg/g), but the values are still well above typical mantle olivine (<0.1 µg/g; Kent and Rossman, 2002). The samples also show a large range in $\delta^{11}B$ values from -11 to +3‰, although the majority fall between -8 and 0‰ (**Fig. 3**). Boron contents are correlated to olivine texture: cores of remnant primary mantle olivine have low B (0.4-7 µg/g) and $\delta^{11}B$ values (-10 to -3‰), whereas olivine rims and fine-grained olivine neoblasts have higher B (3-27 µg/g) and somewhat higher $\delta^{11}B$ values (-7 - +2‰).

Antigorite also has a wide range of B concentrations (2-22 µg/g), which are generally higher than co-existing olivine, except for sample HSS73. $\delta^{11}B$ values overlap with but are on average higher than co-existing olivine (-4 to +6‰). Late-stage lizardite have highest B (17-117 µg/g) and a limited range of $\delta^{11}B$ (mostly -2 to -4‰, some values up to +4‰).

Bulk rock FME concentrations prior to late-stage lizardite veining were calculated based on average compositions of minerals and their modes (see Electronic Supplement). They show a narrow range of Li (1.3-2.4 µg/g), which are typical values for mantle peridotites, a large range in B (2-9 µg/g) which are considerably higher than typical mantle peridotite (<0.1 µg/g B), and highly variable F contents ranging from close to typical mantle peridotite value of ~ 12 µg/g (Kendrick et al., 2017) to >100 µg/g. Chlorine contents show a narrow range (3-10 µg/g) with primary mantle having ca. 5 µg/g (Kendrick et al., 2017). No correlation between any of the FME is apparent.

DISCUSSION

Boron-rich olivine forms in the presence of B-rich fluids such as those derived from dehydration of serpentinite or sediments (Clarke et al., 2020; De Hoog et al., 2014; Scambelluri et al., 2019; Tenthorey and Hermann, 2004). High B contents are very rare for primary olivine in mantle peridotite, and have so far only been reported from a section of the Oman ophiolite which incorporated fluids from the metamorphic sole during nascent subduction in a shallow fore-arc setting at depths of <30 km (Prigent et al., 2018). High B olivine was also reported in the Sapat ultramafic body from the Kohistan arc, Pakistan, but its paragenesis remains unclear (Bouilhol et al., 2009).

The presence of hydrous minerals (antigorite) and zoning of B in olivine from HA peridotites indicate fluid-derived B. Zoning can form during crystal growth, but this is not supported by the sample textures and deformation history. The presence of olivine neoblasts with high B indicates incorporation of B during deformation-induced grain-size reduction.

Zoning in porphyroclasts is therefore likely due to diffusion of B into the crystals during fluid infiltration.

The deformation history of HA and sample microtextures provide constraints on the timing of fluid infiltration. The D1 stage producing preferred orientation of olivine under dry hot conditions took place during mantle flow in the mantle wedge (Mizukami and Wallis, 2005). Olivine porphyroclasts in our samples are remnants of this stage.

Early D2a deformation produced olivine neoblasts with a preferred crystal orientation indicative of H_2O-rich conditions (Mizukami and Wallis, 2005; Wallis et al., 2011) but at temperatures too high to stabilize antigorite (>650 °C). Some porphyroclasts contain abundant fluid inclusions with subduction-related noble gas signatures related to this event (Sumino et al., 2010). Boron in olivine from essentially anhydrous dunite HC123 was introduced during this event, and probably also explains low-B cores in olivine porphyroclasts in other samples (**Fig. 2**). Olivine in HC123 does not contain fluid inclusions, which suggests that B entered olivine via diffusion, not cracking and sealing of fractures.

Further deformation and re-crystallization after T dropped below 650°C induced crystallization of antigorite (stage D2b; Mizukami and Wallis, 2005), which requires significant amounts of water. This event most likely produced B-enriched rims on olivine porphyroclasts as well as B-rich olivine neoblasts. This is supported by B contents of antigorite, which are similar to neoblasts and olivine rims, as expected for $D_B^{ol/atg}$ of 1.0-1.2 (Clarke et al., 2020). Only sample HC123 escaped this event, as evidenced by its lack of antigorite and B-rich olivine rims.

Late-stage veinlets of lizardite are present in three samples (HC87, HC123, HSS46), and all samples except HSS73 also show alteration of grain boundaries and fractures in olivine. The veinlets have considerably higher B contents than other phases. We discount the possibility that all B in these rocks was derived during this late-stage overprint based on sample HSS73, which has very little late-stage alteration, but similarly high B in olivine (5-15 µg/g) as more altered samples. Furthermore, olivine grains adjacent to B-rich lizardite veins are not enriched in B compared to olivine away from such veins, including porphyroclasts with only 2 ppm B dissected by such veins (sample HSS46). Finally, closure temperatures for diffusion for olivine in these samples are ca. 600°C based on trace element and Fe-Mg exchange thermometry (see Electronic Supplement for details), whereas lizardite veining occurred at T <400°C, ruling out B diffusion.

FLUID SOURCES

Boron isotopes provide constraints on fluids sources. Shallow mantle wedge serpentinites have high $\delta^{11}B$ (> +10‰) (Savov et al., 2004), whereas lower $\delta^{11}B$ values (< +5‰) were observed in serpentinites from the deep mantle wedge, as slab-derived fluids become increasingly lower in $\delta^{11}B$ with increasing slab depth (Martin et al., 2016). The B isotope values for olivine of the HA body correspond to slab fluids from 90-120 km depth (Scambelluri and Tonarini, 2012; Yamada et al., 2019), consistent with its estimated P-T conditions (Enami et al., 2004; Guild et al., 2020).

Cores of olivine porphyroclasts have lower B content and $\delta^{11}B$ than their rims (-10 to -3‰ vs. -7 to +2‰, respectively), which suggests an increase in fluid $\delta^{11}B$ during ascent of the HA body in the subduction channel, consistent with the expected systematic increase in $\delta^{11}B$ with shallowing slab depth. The difference in $\delta^{11}B$ between cores and rims/neoblasts would be consistent with a difference in depth of several tens of kilometers (Scambelluri and Tonarini, 2012). Antigorite has somewhat higher $\delta^{11}B$ than olivine rims, which may suggest that it formed at even shallower depth, but equilibrium B isotope fractionation between antigorite and olivine is uncertain due to their poorly constrained site occupations (Muir et al., 2022).

Alternatively, the change in B isotopic composition of olivine cores vs. rims and antigorite reflects a change in the distance from the fluid source, as a sharp decline in B isotope values of over 20‰ was observed in the Oman ophiolite over distances of only several hundred meters (Prigent et al., 2018). However, we observe no spatial correlation with B isotopes for the HA body, which stretches over several kms. Although we cannot exclude B fractionation of fluids during transport from the slab to the HA body whilst it was entrained at depth in the subduction channel, it did not experience the extreme isotope fractionation observed in the Oman ophiolite.

Our proposed interpretation, deep slab fluids infiltrating the HA peridotites, is supported by Cl concentration data. Bulk rock Cl data by Sumino et al. (2010) showed that most samples had 10-20 µg/g Cl, including those with late-stage lizardite, which is the most Cl-rich phase (70-930 µg/g, Table S2). The values are similar to our recalculated bulk Cl contents (4-10 µg/g; Table S1) which exclude lizardite, and close to depleted mantle values (5 ppm Cl; Kendrick et al., 2017). Thus, slab-derived fluids affected the HA body had low salinity, even though they have preserved seawater-derived halogen and noble gas signatures (Sumino et al., 2010). For comparison, eclogite-facies antigorite serpentinites from Erro Tobbio, Italy, and chlorite harzburgites from Almirez, Spain, have high Cl, 200-400 µg/g, and have therefore been interpreted as serpentinites hydrated on seafloor (John et al., 2011; Kendrick et al., 2013). As slab-hosted halogens except F are largely released at shallow depths (Kendrick et al., 2013), the low Cl content of our samples is consistent with infiltration of the HA body by deep slab-derived fluids.

IMPLICATIONS

Boron is released from subducting slabs to the overlying mantle wedges at various depths. Our study of mantle olivine in the HA body shows that primary mantle olivine scavenged B from slab-derived fluids at sub-arc depths (90-120 km) through diffusion and dynamic recrystallization in a subduction channel. Thus, we can infer that the high affinity of B for olivine will result in progressive depletion of B away from the slab, and little if any B would reach the magma source region via porous fluid flow through the olivine-dominated mantle wedge. To explain the high B contents and high δ^{11}B of arc magmas, B must be transported with limited interaction with surrounding peridotite, e.g., through channeled flow (Pirard and Hermann, 2015) or, alternatively, by diapiric movements due to gravitational instabilities of mélange (Marschall and Schumacher, 2012).

Mantle wedge peridotites can be subducted along with oceanic slabs and thus potentially transport B and other FME to the deeper mantle. However, OIBs show very limited evidence for deep B recycling (Hartley et al., 2021; Walowski et al., 2021), which is consistent with only small volumes of mantle wedge peridotites being B-enriched, and points again to highly focused and efficient B transport to arc magma source regions.

ACKNOWLEDGEMENTS

This work was partially supported by the NERC 'Deep Volatiles' consortium (NE/ M000427/1) and NERC-IMF grants (IMF571/ 1015, IMF595/0516), and NSERC Discovery Grant 'Subduction Zone Geochemistry'. We thanks Chris Hayward for his assistance with EPMA, three anonymous reviewers for helpful comments on an earlier version of this manuscript, and Rob Strachan for editorial handling.

FIGURE CAPTIONS

Figure 1. Geological map of the Higashi-akaishi ultramafic body showing sample locations.

Figure 2. Reflective light microscope image of thin section (sample HC87) showing an olivine porphyroclast (outline indicated by dashed line) and surrounding neoblasts. Values

are B concentrations (μg/g) and associated $\delta^{11}B$ values if available. Blue font indicates isotope analysis points, other points are from volatile analysis. Large round spots are LA-ICP-MS pits. ol = olivine, chr = chromite, atg = antigorite, lzd = lizardite

Figure 3. Boron concentrations and isotopic compositions of olivine and serpentine for all (top left panel) and individual samples. Beneath the sample labels are indicated modal abundance of olivine (ol) and antigorite (atg) for the samples, prior to later lizardite overprint. Letters in olivine symbols denote position of analytical spots: C = olivine core, R = olivine rim, I = in-between core and rim, N = neoblast. Dotted lines between symbols indicate analyses from the same olivine. Dashed line in the upper left panel shows modelled compositions of slab-derived fluids at various depths (Scambelluri and Tonarini, 2012) plotted at four times lower B concentration. Yellow rectangle in the upper left panel shows B content and isotopic composition of olivine from Depleted MORB mantle (DMM) (Marschall et al., 2017).

Figure 4. Schematic diagram showing the history of HA body. (1) Ultramafic body from crust-mantle transition sagged into the mantle wedge and (2A) was dragged down by mantle flow towards the subduction interface and fluxed by slab-derived fluids, which led to the diffusion of B into olivine; (2B) Antigorite serpentine started to form by hydration of olivine during exhumation in the subduction channel, when the body cooled to below 650°C whilst still at high pressure; (3) late-stage B-rich lizardite veins formed during or after incorporation into the Sanbagawa Belt.

[1]Supplemental Material contains analytical methods, sample descriptions including trace element geochemistry (2 tables and 1 figure), and SIMS spot locations on the samples. Please visit https://doi.org/10.1130/XXXX to access the supplemental material, and contact editing@geosociety.org with any questions.

REFERENCES CITED

Aoya, M., Endo, S., Mizukami, T., and Wallis, S. R., 2013, Paleo-mantle wedge preserved in the Sambagawa high-pressure metamorphic belt and the thickness of forearc continental crust: Geology, v. 41, no. 4, p. 451-454, 10.1130/G33834.1

Ayers, J., 1998, Trace element modeling of aqueous fluid - peridotite interaction in the mantle wedge of subduction zones: Contributions to Mineralogy and Petrology, v. 132, no. 4, p. 390-404, 10.1007/s004100050431

Bouilhol, P., Burg, J.-P., Bodinier, J.-L., Schmidt, M. W., Dawood, H., and Hussain, S., 2009, Magma and fluid percolation in arc to forearc mantle: Evidence from Sapat (Kohistan, Northern Pakistan): Lithos, v. 107, no. 1-2, p. 17-37, 10.1016/j.lithos.2008.07.004

Clarke, E., De Hoog, J. C. M., Kirstein, L. A., Harvey, J., and Debret, B., 2020, Metamorphic olivine records external fluid infiltration during serpentinite dehydration: Geochemical Perspectives Letters, v. 16, p. 25-29, 10.7185/geochemlet.2039

De Hoog, J. C. M., Hattori, K., and Jung, H., 2014, Titanium- and water-rich metamorphic olivine in high-pressure serpentinites from the Voltri Massif (Ligurian Alps, Italy): evidence for deep subduction of high-field strength and fluid-mobile elements: Contributions to Mineralogy and Petrology, v. 167, no. 3, p. Artn 990, 10.1007/S00410-014-0990-X

De Hoog, J. C. M., and Savov, I. P., 2018, Boron Isotopes as a Tracer of Subduction Zone Processes, in Marschall, H., and Foster, G., eds., Boron Isotopes: The Fifth Element: Cham, Springer International Publishing, p. 217-247.

Enami, M., Mizukami, T., and Yokoyama, K., 2004, Metamorphic evolution of garnet-bearing ultramafic rocks from the Gongen area, Sanbagawa belt, Japan: Journal of Metamorphic Geology, v. 22, no. 1, p. 1-15, 10.1111/j.1525-1314.2003.00492.x

Guild, M. R., Till, C. B., Mizukami, T., and Wallis, S., 2020, Petrogenesis of the Higashi-Akaishi Ultramafic Body: Implications for Lower Crustal Foundering and Mantle Wedge Processes: Journal of Petrology, v. 61, no. 9, 10.1093/petrology/egaa089

Hartley, M. E., de Hoog, J. C. M., and Shorttle, O., 2021, Boron isotopic signatures of melt inclusions from North Iceland reveal recycled material in the Icelandic mantle source: Geochimica Et Cosmochimica Acta, v. 294, p. 273-294, 10.1016/j.gca.2020.11.013

Hattori, K., Wallis, S., Enami, M., and Mizukami, T., 2010, Subduction of mantle wedge peridotites: Evidence from the Higashi-akaishi ultramafic body in the Sanbagawa metamorphic belt: Island Arc, v. 19, no. 1, p. 192-207, 10.1111/j.1440-1738.2009.00696.x

Hattori, K. H., and Guillot, S., 2003, Volcanic fronts form as a consequence of serpentinite dehydration in the forearc mantle wedge: Geology, v. 31, no. 6, p. 525-528,

John, T., Scambelluri, M., Frische, M., Barnes, J. D., and Bach, W., 2011, Dehydration of subducting serpentinite: Implications for halogen mobility in subduction zones and the deep halogen cycle: Earth and Planetary Science Letters, v. 308, no. 1-2, p. 65-76,

Kendrick, M. A., Hemond, C., Kamenetsky, V. S., Danyushevsky, L., Devey, C. W., Rodemann, T., Jackson, M. G., and Perfit, M. R., 2017, Seawater cycled throughout Earth/'s mantle in partially serpentinized lithosphere: Nature Geosci, v. 10, no. 3, p. 222-228, 10.1038/ngeo2902

Kendrick, M. A., Honda, M., Pettke, T., Scambelluri, M., Phillips, D., and Giuliani, A., 2013, Subduction zone fluxes of halogens and noble gases in seafloor and forearc serpentinites: Earth and Planetary Science Letters, v. 365, p. 86-96, 10.1016/j.epsl.2013.01.006

Kent, A. J. R., and Rossman, G. R., 2002, Hydrogen, lithium, and boron in mantle-derived olivine: The role of coupled substitutions: American Mineralogist, v. 87, no. 10, p. 1432-1436,

Marschall, H. R., and Schumacher, J. C., 2012, Arc magmas sourced from melange diapirs in subduction zones: Nature Geoscience, v. 5, no. 12, p. 862-867, 10.1038/Ngeo1634

Marschall, H. R., Wanless, V. D., Shimizu, N., von Strandmann, P. A. E. P., Elliott, T., and Monteleone, B. D., 2017, The boron and lithium isotopic composition of mid-ocean ridge basalts and the mantle: Geochimica Et Cosmochimica Acta, v. 207, p. 102-138, 10.1016/j.gca.2017.03.028

Martin, C., Flores, K. E., and Harlow, G. E., 2016, Boron isotopic discrimination for subduction-related serpentinites: Geology, v. 44, no. 11, p. 899-902, 10.1130/G38102.1

Mizukami, T., Ishigami, S., and Arai, S., 2012, Topotaxic replacement of olivine by a lizardite and brucite mixture in the Higashi-akaishi ultramafic body, Japan Geoscience Union Meeting, Japan Geoscience Union,

Mizukami, T., and Wallis, S. R., 2005, Structural and petrological constraints on the tectonic evolution of the garnet-lherzolite facies Higashi-akaishi peridotite body, Sanbagawa belt, SW Japan: Tectonics, v. 24, no. 6, p. Artn Tc6012, 10.1029/2004tc001733

Muir, J. M. R., Chen, Y., Liu, X., and Zhang, F., 2022, Extremely Stable, Highly Conductive Boron-Hydrogen Complexes in Forsterite and Olivine: Journal of Geophysical Research: Solid Earth, v. 127, no. 6, 10.1029/2022jb024299

Pirard, C., and Hermann, J., 2015, Focused fluid transfer through the mantle above subduction zones: Geology, v. 43, no. 10, p. 915-918, 10.1130/g37026.1

Prigent, C., Guillot, S., Agard, P., Lemarchand, D., Soret, M., and Ulrich, M., 2018, Transfer of subduction fluids into the deforming mantle wedge during nascent subduction:

Evidence from trace elements and boron isotopes (Semail ophiolite, Oman): Earth and Planetary Science Letters, v. 484, p. 213-228, 10.1016/j.epsl.2017.12.008

Savov, I. P., Tonarini, S., Ryan, J., and Mottl, M. J., Boron isotope geochemistry of serpentinites and porefluids from Leg 195, Site 1200, S.Chamorro Seamount, Mariana forearc region (abstract), in Proceedings International Geological Congress, Florence, Italy, 2004.

Scambelluri, M., Cannao, E., and Gilio, M., 2019, The water and fluid-mobile element cycles during serpentinite subduction. A review: European Journal of Mineralogy, v. 31, no. 3, p. 405-428, 10.1127/ejm/2019/0031-2842

Scambelluri, M., and Tonarini, S., 2012, Boron isotope evidence for shallow fluid transfer across subduction zones by serpentinized mantle: Geology, v. 40, no. 10, p. 907-910, Doi 10.1130/G33233.1

Sumino, H., Burgess, R., Mizukami, T., Wallis, S. R., and Ballentine, C. J., 2007, Subducted noble gas and halogen preserved in wedge mantle peridotite from the Sanbagawa belt, SW Japan: Geochimica Et Cosmochimica Acta, v. 71, no. 15, p. A985-A985,

Sumino, H., Burgess, R., Mizukami, T., Wallis, S. R., Holland, G., and Ballentine, C. J., 2010, Seawater-derived noble gases and halogens preserved in exhumed mantle wedge peridotite: Earth and Planetary Science Letters, v. 294, no. 1-2, p. 163-172, 10.1016/j.epsl.2010.03.029

Tenthorey, E., and Hermann, J., 2004, Composition of fluids during serpentinite breakdown in subduction zones: Evidence for limited boron mobility: Geology, v. 32, no. 10, p. 865-868, Doi 10.1130/G20610.1

Wallis, S. R., Kobayashi, H., Nishii, A., Mizukami, T., and Seto, Y., 2011, Obliteration of olivine crystallographic preferred orientation patterns in subduction-related antigorite-bearing mantle peridotite: an example from the Higashi–Akaishi body, SW Japan:

Geological Society, London, Special Publications, v. 360, no. 1, p. 113-127, 10.1144/sp360.7

Walowski, K. J., Kirstein, L. A., De Hoog, J. C. M., Elliott, T., Savov, I. P., Jones, R. E., and Eimf, 2021, Boron recycling in the mantle: Evidence from a global comparison of ocean island basalts: Geochimica Et Cosmochimica Acta, v. 302, p. 83-100, 10.1016/j.gca.2021.03.017

Yamada, C., Tsujimori, T., Chang, Q., and Kimura, J. I., 2019, Boron isotope variations of Franciscan serpentinites, northern. California: Lithos, v. 334, p. 180-189, 10.1016/j.lithos.2019.02.004

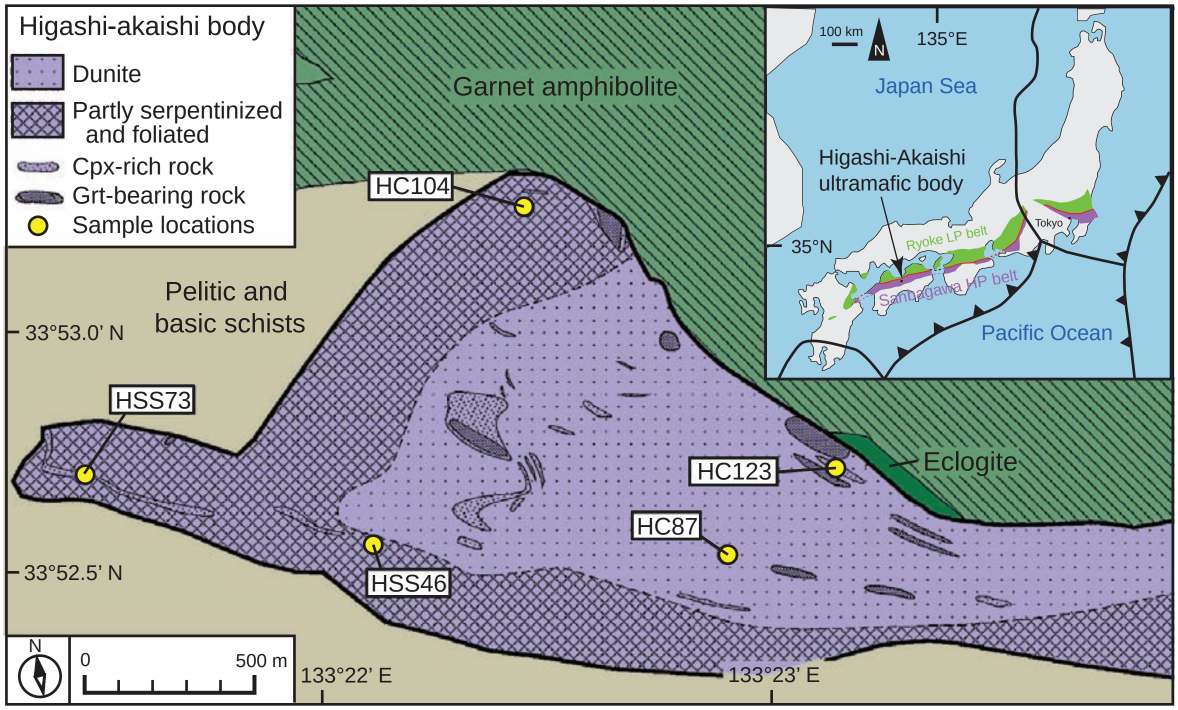
Higashi-akaishi body
Dunite
Partly serpentinized and foliated
Cpx-rich rock
Grt-bearing rock
Sample locations
Garnet amphibolite
Pelitic and basic schists
HC104
HSS73
HSS46
HC123
HC87
Eclogite
33°53.0' N
33°52.5' N
133°22' E
133°23' E
N
0
500 m
100 km
135°E
Japan Sea
Higashi-Akaishi ultramafic body
35°N
Ryoke LP belt
Sanbagawa HP belt
Tokyo
Pacific Ocean

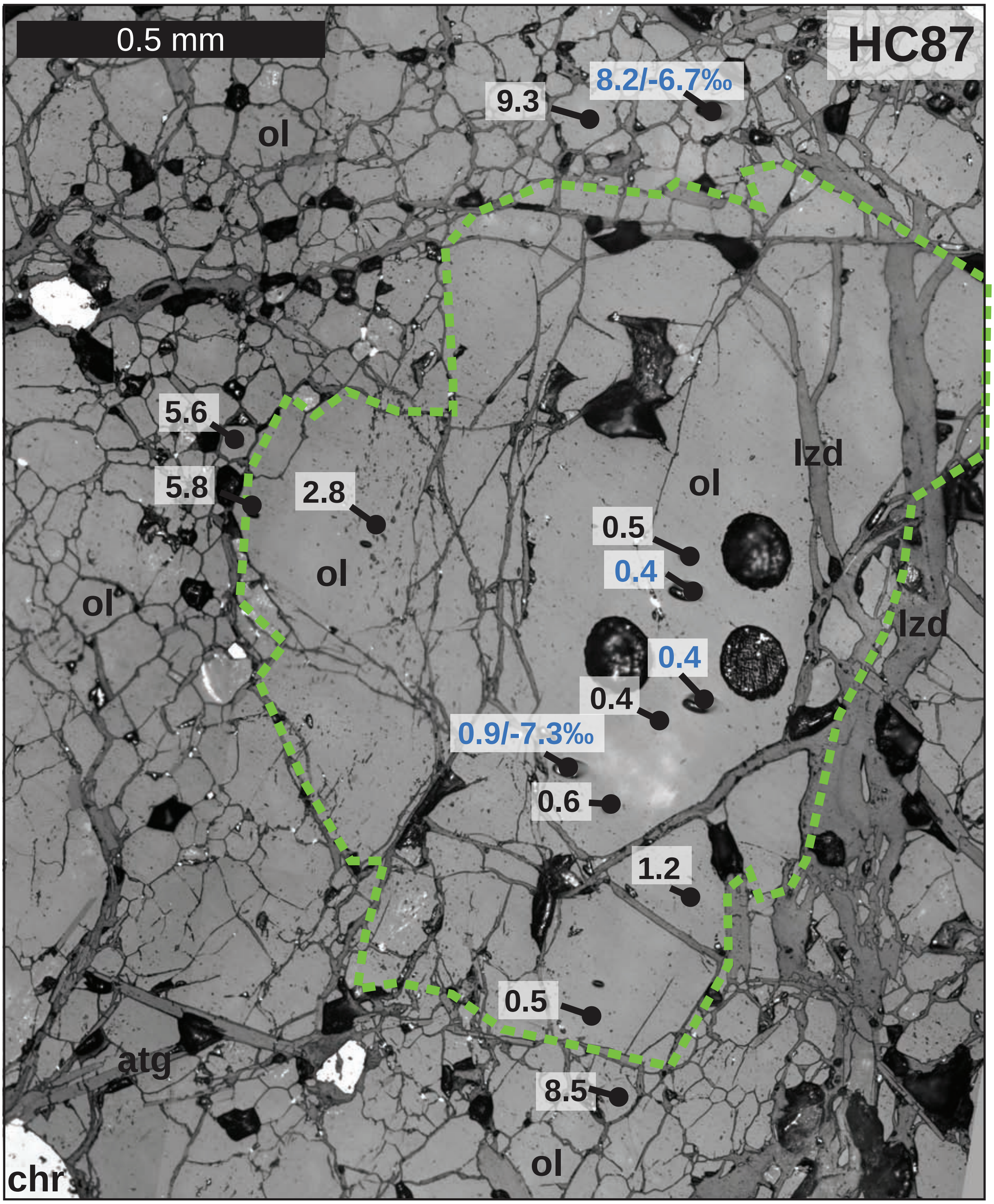
0.5 mm
HC87
9.3
8.2/-6.7‰
ol
5.6
5.8
2.8
ol
ol
ol
lzd
0.5
0.4
lzd
0.4
0.4
0.9/-7.3‰
0.6
1.2
0.5
atg
8.5
ol
chr

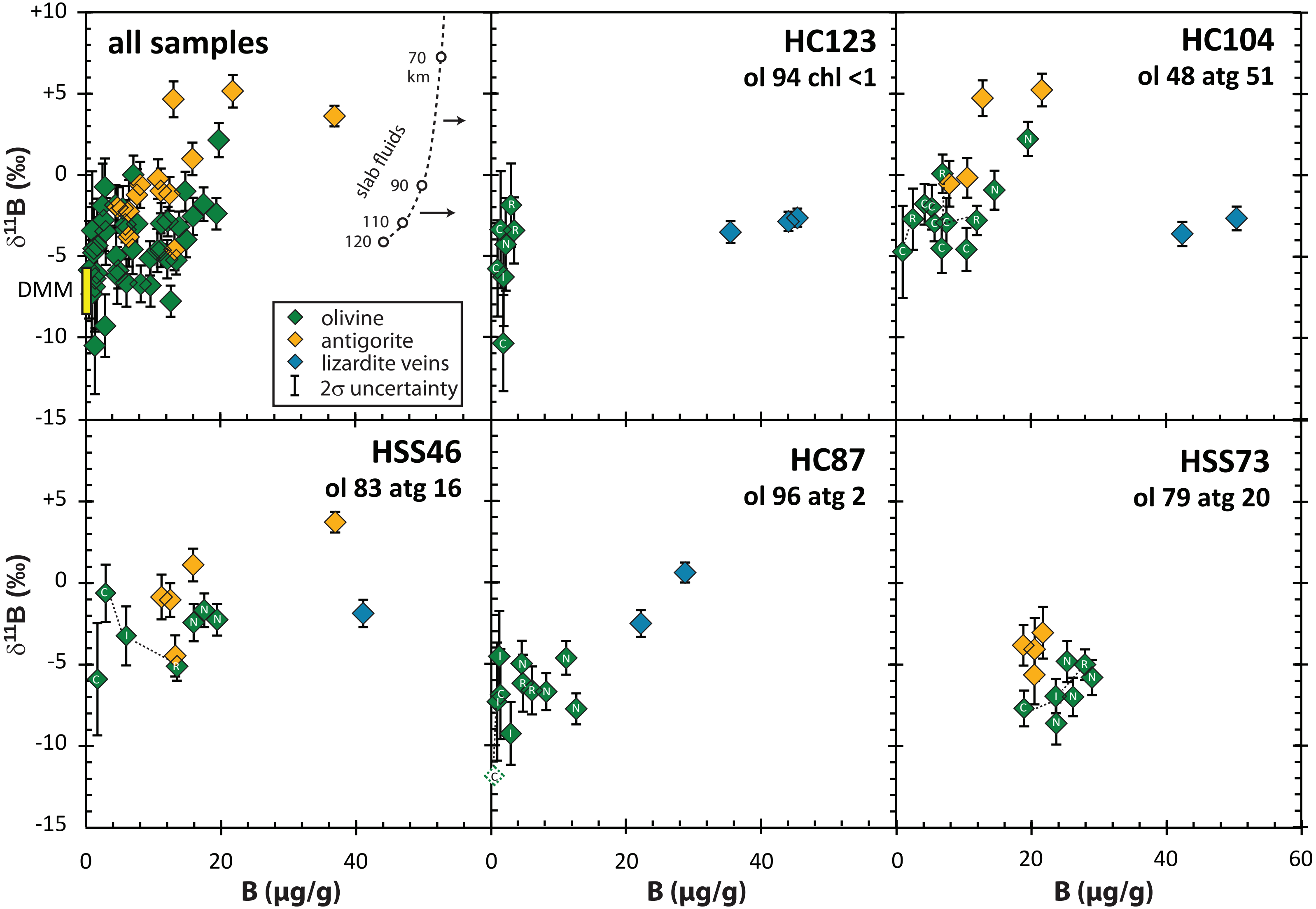
all samples
HC123
ol 94 chl <1
HC104
ol 48 atg 51
HSS46
ol 83 atg 16
HC87
ol 96 atg 2
HSS73
ol 79 atg 20
slab fluids
70 km
90
110
120
DMM
olivine
antigorite
lizardite veins
2σ uncertainty
δ11B (‰)
B (μg/g)
+10
+5
0
-5
-10
-15
0
20
40
60

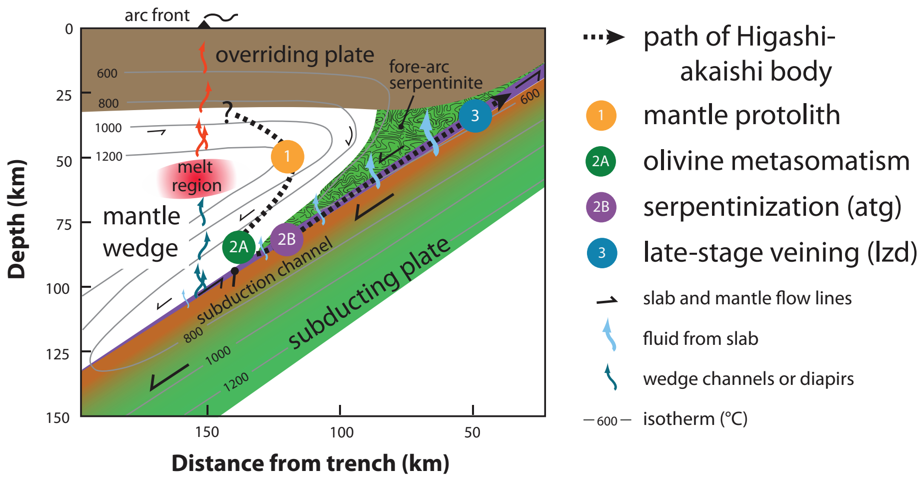

arc front
overriding plate
fore-arc serpentinite
melt region
mantle wedge
subduction channel
subducting plate
Depth (km)
Distance from trench (km)
0
25
50
75
100
125
150
150
100
50
600
800
1000
1200
?
1
2A
2B
3
path of Higashi-akaishi body
mantle protolith
olivine metasomatism
serpentinization (atg)
late-stage veining (lzd)
slab and mantle flow lines
fluid from slab
wedge channels or diapirs
isotherm (°C)

Analytical methods

Fluid-mobile elements (FME: Li, B, F, Cl) concentrations and B isotope ratios of olivine were measured in-situ in thick (~ 50 μm) sections by Secondary Ion Mass Spectrometry (SIMS) at the Edinburgh Ion Microprobe Facility using a Cameca IMS-4f and a Cameca IMS-1270, respectively, following the methods detailed in Supplementary Information of Clarke et al. (2020). Boron isotope measurements of olivine and serpentine were calibrated using matrix-matched standards.

A small LA-ICP-MS dataset of olivine, serpentine and chromite in the same samples was obtained using a Thermo Element II with a NewWave Excimer laser system at Oxford University following the methods in De Hoog et al. (2010), which provided additional trace elements.

Electron microprobe data for the samples was presented by Hattori et al. (2010) and was supplemented by a small number of analyses using a Cameca SX100 at the University of Edinburgh, see Clarke et al. (2020) for analytical details.

Sample descriptions (petrography and B contents)

Table S1. Brief sample descriptions

Sample	Rock type	Assemblage [a]	Texture	Late-stage overprint
HC123	Dunite	Ol 94, Cr 6, Chl <1	Fine grained, disseminated chromite	Pervasive, extensive veining (ca. 20%)
HC87	Atg dunite	Ol 96, Atg 2, Cr 1.5	Porphyroclastic	Pervasive, extensive veining (ca 45%)
HSS46	Atg dunite	Ol 83, Atg 16, Cr 1	Porphyroclastic	Extensive veining, mesh (ca. 40%)
HSS73	Atg dunite	Ol 79, Atg 20, Cr 1	Fine grained, foliated	Nearly absent, no veining
HC104	Atg serpentinite	Ol 48, Atg 51, Cr 1	Porphyroclastic, foliated	Limited to grain boundaries (ca. 10%)

[a] Mineral assemblage prior to late-stage overprint. Atg = antigorite, Cr = chromite, Ol = olivine, Chl = chlorite

HC123: Fine-grained (some larger grains highly fractured) olivine with no antigorite but rare chlorite flakes, slightly oriented, abundant chromite in large fine-grained seams and patches, pervasive late-stage veining of lizardite (several mm in width) cross-cutting the matrix. Olivine: Low B (avg 2 μg/g), δ^{11}B ca. -4 excl 1 outlier of -10. Small concentration range (1-5 μg/g). The sample also contains chlorite as small grains in the matrix, but no antigorite. Extensive late-stage veining with high B (32-117 μg/g).

HC87: Fairly coarse-grained with sparse small blades of antigorite (<2 modal%) and no apparent foliation. Not always clear what are fractured remnants of large grains or neoblasts. Very pervasive late-stage veining in multiple generations affecting much of the samples but large unaltered patches are present. Large porphyroclastic olivine most have large amounts of small needle-like inclusions, probably serpentine. Olivine has large variation in B contents with large (> 150 μm) grains having fairly uniform low B (0.5-1 μg/g) with slight increase from core to rim (up to 6 μg/g), but smaller grains have ca. 8-13 μg/g. No correlation with proximity to wide lizardite veins.

HSS46: (near the serpentinite border) Generally fine-grained with some patches of coarse olivine and large (several mm) antigorite blades (ca. 20% overall). Very pervasive late-stage veining and mesh of lizardite . Chromite with magnetite rims. No strong foliation. Olivine is mostly fine-grained but a large 2mm porphyroclasts show core to rim zoning of B (2-16 μg/g). Another porphyroclstic olivine grain, containing lizardite mesh has low B (2 μg/g) even though it's directly adjacent to mesh with 24 μg/g B. Antigorite has 9-38 μg/g B.

HSS73: strong foliation, nearly completely neoblastic olivine (range ca. 100-250 μm) apart from several relict mm-sized porphyroclasts, abundant fine antigorite needles (ca. 10%), very limited late overprint with no veining having developed. Olivine: three core-rim B profiles although only one with isotopes. Cores have low B but vary (two grains 5-7 μg/g, one other only 1.5 μg/g), but rims are similar and also similar to neoblasts (10-15 μg/g). Note that the sample has abundant antigorite needles but no lizardite veining, providing strong evidence that B in olivine is not a late-stage overprint.

HC104: strongly foliated, but abundant large olivine porphyroclasts. Pervasive fine-grained antigorite needles with some coarse-grained (>1 mm) locally, often segregating into veins/bundles (ca. 30% overall). Late-stage veining limited, lizardite mostly fills cracks in olivine and grain boundaries in matrix. Olivine B: 3 core-rim points 200-400 μm apart. Data quite variable for cores and rims, although generally B goes up. The low core concentration (1 μg/g B) is from a lasered grain, but the rim is uncertain, big discrepancy between 4f and 1270 (12 vs 2.5 μg/g). Two other grain have higher cores (5-7 μg/g) but core-rim less clear for one. The other one was previously lasered (two holes, data identical) but little B variation. Neoblasts variable but high and cover range of rims (8-20 μg/g B).

We did not determine serpentine polysomes as part of this study, but base our distinction of antigorite vs. lizardite on observations of similar samples from the literature (Mizukami et al., 2012; Mizukami et al., 2004; Sumino et al., 2010; Wallis et al., 2011).

Mineral trace elements and thermobarometry

<u>Olivine</u>

All samples contain primary mantle olivine (Fo90-94). Concentrations of trace elements in olivine of various metals such as Sc (1-3 μg/g), MnO 0.10-0.12 wt.%), NiO (0.35-0.38 wr.%), Zn (10-40 μg/g) and Co (110-140 μg/g) are typical of mantle peridotites although Cu contents (ca. 0.1μg/g) appear low (De Hoog et al., 2010).

Temperature-sensitive elements in olivine, such as Na (<10 μg/g), Al (<4 μg/g), Ca (20-40 μg/g), V <0.5 μg/g) and Cr (4-10 μg/g) are extremely low, equivalent to equilibration at ca. 600 °C (De Hoog et al., 2010), which most likely represents closure temperatures during slow cooling of the body. Titanium contents are typical values of depleted spinel peridotites but vary per sample, with olivine in HC123 (20-70 μg/g) markedly higher Ti than olivine in the other samples (<10 μg/g). Low Y contents (<0.01 μg/g) and Zr (<0.025 μg/g) are consistent with the highly residual nature of the dunites. In contrast, Li contents (**Fig. S1**) are typical of mantle olivine, with HC123 and HC104 having somewhat higher Li (2-4 µg/g) than other samples (ca. 1.5 µg/g). These two samples also have high F contents (HC123: 40-70 µg/g; HC104: 6-30 µg/g) compared to other samples (mostly 1-10 µg/g) (**Fig. 2**). Boron concentrations are variable and significantly above typical mantle olivine value <0.1 µg/g (Kent and Rossman, 2002). The two most B-enriched samples (HC104 and HSS73) are also high in Cl (>6 vs <5 µg/g for other samples) (**Fig. S1**).

Antigorite occurring as small lath-shaped crystals in the sample matrix have high Mg# (0.95-0.97), high Al_2O_3 (0.2-1.1 wt%) and variably Cr (0.03-0.44 wt%), which indicates that the partial breakdown of chromite may be involved in its formation. Lithium contents are very low (<0.2 µg/g), which is common in subduction-related serpentinites (e.g., Clarke et al., 2020). It has low Cl contents (generally <30 µg/g) and generally low F (<100 µg/g) except in sample HC104 which has ca. 250 µg/g F. Antigorite also has notably high As (0.7-2 µg/g) and Sb (0.2-0.3 µg/g).

Chlorite was only observed in antigorite-free sample HC123, where is occurs as rare small flakes in the matrix. It is characterised by high Ti (100-150 µg/g), high F (400-600 µg/g) but low Cl contents (30-100 µg/g). Boron contents are similar to olivine from the same sample (1-5 µg/g).

In comparison to antigorite, lizardite has low Al (0.002-0.10 wt.%) and Cr (<0.001 wt.), and low As and Sb but somewhat higher Li. Apart from HC123, samples have elevated Li (0.5-2 µg/g) in lzd veins compared to atg. Lizardite veins have elevated Cl (60-900 µg/g) compared to atg, but are highly variable, up to an order of magnitude in most samples. Some lzd veins (HC123, HC104) also have high F but its variable and does not correlate with Cl.

Chromite compositions are similar in all samples, with high Cr# (0.7-0.8) and low Mg# (0.3-0.5). Sample HC123 has somewhat high TiO_2 (0.4 wt.%) compared to other samples (0.04-0.14 wt%) with somewhat lower V and Sc contents.

Spinel-olivine thermometry of Ballhaus et al. (1991) for sample HC123 yields 670°C (Ballhaus et al., 1991) This is a typical value for spinel-olivine pairs from slowly exhumed terranes (e.g., Chen et al., 2020; De Hoog et al., 2009) and represents the temperature when Fe-Mg exchange between olivine and spinel becomes so slow that it no further re-equilibrates during cooling of the rock (i.e., a closure temperature rather than equilibration temperature). The oxygen fugacity is high (ΔNNO + 1.5).

Table S2. Calculated bulk rock FME contents (excluding secondary overprint)

sample	Li (µg/g)	1s	B (µg/g)	1s	F (µg/g)	1s	Cl (µg/g)	1s
HC123	2.4	± 0.2	2.1	± 0.3	52	± 3	3.3	± 0.4
HC87	1.4	± 0.1	3.9	± 1.1	8.2	± 1.2	4.8	± 1.5
HSS46	1.3	± 0.1	4.9	± 0.6	15	± 2	4.8	± 1.2
HSS73	1.4	± 0.3	9.4	± 1.9	13	± 2	9.9	± 3.8
HC104	1.8	± 0.2	9.1	± 1.1	138	± 2	9.4	± 2.0

1s uncertainties based on propagated uncertainties of multiple analyses of mineral grains and mineral modes.

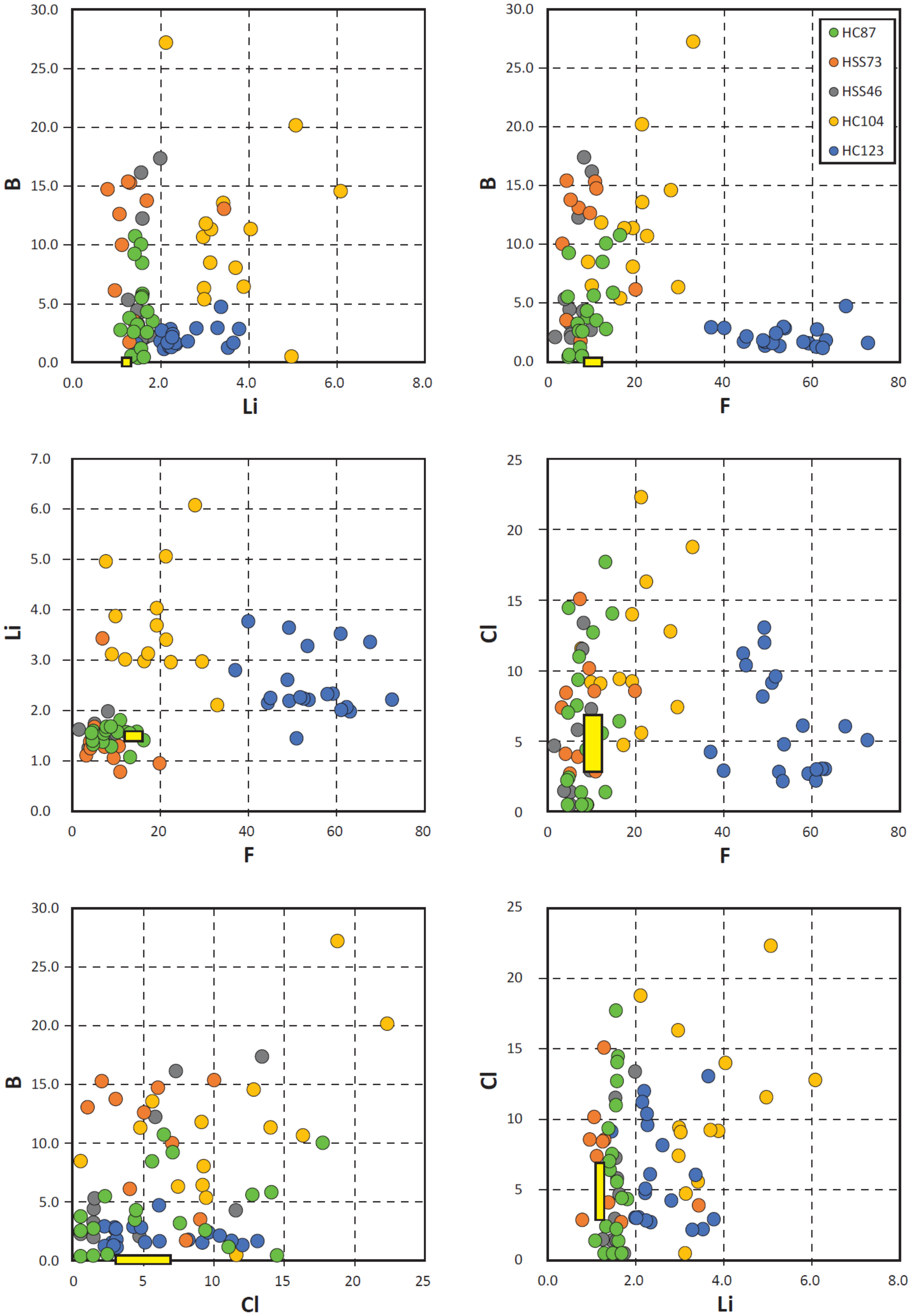

Fig. S1 Fluid-mobile element (Li, B, F, Cl) systematics of olivine in Higashi-akaishi metaperidotites. The composition of average depleted mantle ±1s is indicated by a yellow rectangle (Kendrick et al., 2017; Marschall et al., 2017).

References

Ballhaus, C., Berry, R. F., and Green, D. H., 1991, High-pressure experimental calibration of the olivine-ortho-pyroxene-spinel oxygen geobarometer - Implications for the oxidation-state of the upper mantle: Contributions to Mineralogy and Petrology, v. 107, no. 1, p. 27-40,

Chen, C., De Hoog, J. C. M., Su, B.-X., Wang, J., Uysal, İ., and Xiao, Y., 2020, Formation process of dunites and chromitites in Orhaneli and Harmancık ophiolites (NW Turkey): Evidence from in-situ Li isotopes and trace elements in olivine: Lithos, v. 376-377, p. 105773, 10.1016/j.lithos.2020.105773

Clarke, E., De Hoog, J. C. M., Kirstein, L. A., Harvey, J., and Debret, B., 2020, Metamorphic olivine records external fluid infiltration during serpentinite dehydration: Geochemical Perspectives Letters, v. 16, p. 25-29, 10.7185/geochemlet.2039

De Hoog, J. C. M., Gall, L., and Cornell, D. H., 2010, Trace-element geochemistry of mantle olivine and application to mantle petrogenesis and geothermobarometry: Chemical Geology, v. 270, no. 1-4, p. 196-215, DOI 10.1016/j.chemgeo.2009.11.017

De Hoog, J. C. M., Janak, M., Vrabec, M., and Froitzheim, N., 2009, Serpentinised peridotites from an ultrahigh-pressure terrane in the Pohorje Mts. (Eastern Alps, Slovenia): Geochemical constraints on petrogenesis and tectonic setting: Lithos, v. 109, no. 3-4, p. 209-222,

Hattori, K., Wallis, S., Enami, M., and Mizukami, T., 2010, Subduction of mantle wedge peridotites: Evidence from the Higashi-akaishi ultramafic body in the Sanbagawa metamorphic belt: Island Arc, v. 19, no. 1, p. 192-207, 10.1111/j.1440-1738.2009.00696.x

Kendrick, M. A., Hemond, C., Kamenetsky, V. S., Danyushevsky, L., Devey, C. W., Rodemann, T., Jackson, M. G., and Perfit, M. R., 2017, Seawater cycled throughout Earth/'s mantle in partially serpentinized lithosphere: Nature Geosci, v. 10, no. 3, p. 222-228, 10.1038/ngeo2902

Kent, A. J. R., and Rossman, G. R., 2002, Hydrogen, lithium, and boron in mantle-derived olivine: The role of coupled substitutions: American Mineralogist, v. 87, no. 10, p. 1432-1436,

Marschall, H. R., Wanless, V. D., Shimizu, N., von Strandmann, P. A. E. P., Elliott, T., and Monteleone, B. D., 2017, The boron and lithium isotopic composition of mid-ocean ridge basalts and the mantle: Geochimica Et Cosmochimica Acta, v. 207, p. 102-138, 10.1016/j.gca.2017.03.028

Mizukami, T., Ishigami, S., and Arai, S., 2012, Topotaxic replacement of olivine by a lizardite and brucite mixture in the Higashi-akaishi ultramafic body, Japan Geoscience Union Meeting, Japan Geoscience Union,

Mizukami, T., Wallis, S. R., and Yamamoto, J., 2004, Natural examples of olivine lattice preferred orientation patterns with a flow-normal a-axis maximum: Nature, v. 427, no. 6973, p. 432-436, 10.1038/nature02179

Sumino, H., Burgess, R., Mizukami, T., Wallis, S. R., Holland, G., and Ballentine, C. J., 2010, Seawater-derived noble gases and halogens preserved in exhumed mantle wedge peridotite: Earth and Planetary Science Letters, v. 294, no. 1-2, p. 163-172, 10.1016/j.epsl.2010.03.029

Wallis, S. R., Kobayashi, H., Nishii, A., Mizukami, T., and Seto, Y., 2011, Obliteration of olivine crystallographic preferred orientation patterns in subduction-related antigorite-bearing mantle peridotite: an example from the Higashi–Akaishi body, SW Japan: Geological Society, London, Special Publications, v. 360, no. 1, p. 113-127, 10.1144/sp360.7